Four Contributions to the 3rd Edition of *Accelerator Handbook*

V.Shiltsev (FNAL), G.Franchetti (GSI), G.Sterbini (CERN)

July 23, 2021

Abstract

We present brief summaries "Operational Limits in High-Intensity Hadron Accelerators" (new), "Beam-Beam Compensation Schemes" (update), "Space-Charge Compensation in Hadron Beams" (update) and "Electron Lenses"(update).

This manuscript has been authored by Fermi Research Alliance, LLC under Contract No. DE-AC02-07CH11359 with the U.S. Department of Energy, Office of Science, Office of High Energy Physics.

1 Operational Limits in High-Intensity Hadron Accelerators

V. Shiltsev, FNAL
G. Franchetti, GSI

Operational experience of existing and design studies of proposed hadron (proton, antiproton, H^- and heavier ions) accelerators indicate critical importance of detrimental effects at high beam intensities, such emittance growth, halo formation and particle losses. The former particularly affect luminosity of colliders [1], while the particle losses may result in dysfunctional accelerator components (such as superconducting magnets and RF cavities, electronics in the tunnel, and experimental apparatus) and/or interfere with the needs of operational maintenance of the components of linacs [2], cyclotrons [3] and synchrotrons [4]. As a design guideline for hands-on maintenance, the average beam power loss must be under $W = Ze(dN/dt)E_k \leq 1$ W per meter, equivalent, for example, to the loss of dN/dt=6·10^9 protons/s at 1 GeV. That translates into a level of radioactivation of approximately 1 mSv/h (100 mrem/h), measured at 30 cm from the surface, 4 h after the machine is shut down (see Chapter 8). The corresponding limit for heavy ion beams is somewhat relaxed, e.g., 5W/m or more for uranium beams, depending on the energy and geometry of irradiated accelerator components [5]. Controlled beam losses at specific locations, such as collimators, beam dumps, injection/stripping regions, and beam windows where heavy shielding is provided, can be much higher.

In contrast, uncontrolled losses are not well localized and their magnitude and extent might be difficult to predict and prevent. Some of them are linearly proportional to the beam intensity, such as those due to, e.g., vacuum gas scattering and stripping, Coulomb scattering and nuclear scattering in injection foils, magnetic stripping, kicker misfires, noises in RF systems and magnet power-supply systems, etc. Other types of losses grow progressively with intensity, such as those caused by the space-charge effects, intrabeam stripping, instabilities and electron-cloud effects.

Different types of accelerators are subject to different phenomena and have different limitations associated with high beam intensity operation.

1.1 Linacs

Control of the beam losses has become of critical importance for modern high-intensity H^+ and H^- pulsed and CW linacs, especially superconducting ones [6]. Besides beam losses caused by malfunctioning of accelerator components, errant beam events, such as RF field collapses caused by an arc within cavities or at the vacuum windows - i.e., those that usually can be avoided by better maintenance, advanced control and fast beam shut-off - there are harder to treat collective phenomena, such as space-charge effects.

Non-linear self-fields induce a spread of the particle oscillation frequencies (tunes, in all three directions) from $\eta\nu_0$ to ν_0, where ν_0 is the unperturbed low in-

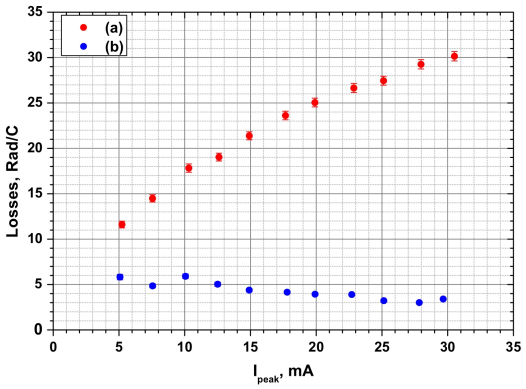

Figure 1: The normalized SNS BLM signals (Rads per transmitted charge) vs peak current for H^- beam (a) and proton beam (b).

tensity value and the intensity dependent tune depression factor (see Sec.2.4.6) that can be as large as $\eta \geq 0.5$. Not only does such a spread transfer any mismatch into the effective emittance growth, but also the beam envelope instabilities can occur when the phase advance per focusing period without space charge is greater than 90° [7, 8] - the latter is usually avoided by proper lattice design. Another effective mechanism leading to losses is parametric resonances in space-charge dominated beams when the single particle tunes and the envelope tunes of the core oscillations are in integer ratio (most often, 2:1) [9]. That results in the energy transfer from the core movement to the single particle excursions to large amplitudes, and formation of a halo. These instabilities can be avoided by proper choice of operational tunes, good matching in the lattice transitions to avoid appreciable halo formation [2], and reduction of the space-charge driven energy exchange between the transverse and longitudinal planes by providing beam equi-partitioning or selection of proper operational area on the Hoffmann chart [8].

A high-intensity beam passing through an RF cavity excites EM modes, which can lead to transverse and longitudinal beam breakup instabilities. While the HOMs were found to be of little importance for the present day highest power SNS linac, the effect can be of concern for more ambitious projects [10].

An operationally dominant uncontrolled beam loss mechanism in high-power H^- linacs is the stripping of loosely bound electrons (with electron affinity of only 0.75 eV) that results in neutral hydrogen ions which are no longer affected by the accelerating and focusing elements. Such stripping can be due to black body radiation, electromagnetic fields, and collisions with residual gas molecules - and in that case, the losses are proportional to the beam current. But even more pronounced are losses due to the stripping caused by the intrabeam collisions (Sec. 2.4.12) which are proportional to the square of the beam intensity - see Fig.1. As the rate of such stripping is proportional to the square of the beam density, the mitigation strategies are based on operating with larger sized beams

by lowering the focusing magnet gradients and increasing physical apertures in all three planes. The rule of thumb for high-intensity linacs is to provide the ratio of the transverse beam aperture to the RMS beam size greater than 12 [2].

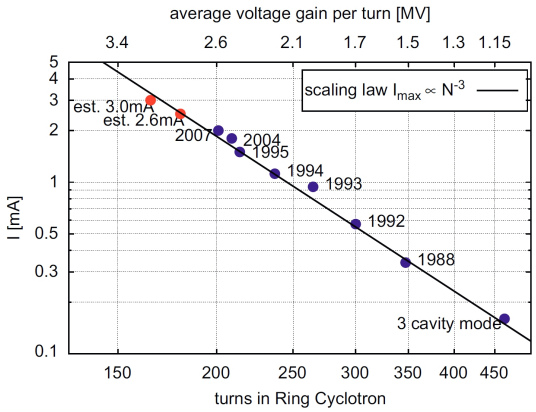

Figure 2: Maximum output current vs the number of turns in the PSI cyclotron.

1.2 Cyclotrons

Cyclotrons accelerating H^- ions have the advantage of achieving very efficient extraction by stripping the ions in a thin carbon foil, but the beam losses due to H^- disruption in strong electromagnetic fields or by collisions with gas molecules impose severe limits on the maximum beam power. The most powerful are, therefore, proton cyclotrons in which the most critical limitations are losses at the electrostatic septum assisted extraction, which have to be kept low in order to avoid damage to the components and to minimize their activation.

Prerequisites for low loss operation are good beam quality and sufficient separation of turns at the extraction radius. For high beam current J, strong longitudinal space-charge forces during the N-turn acceleration in the cyclotron lead to additional energy spread proportional to JN^2, making the ratio of beam width to the turn separation roughly proportional to JN^3 [11]. The resulting scaling of the maximum attainable current:

$$J_{max} \propto \frac{1}{N^3} \propto V_{RF}^3 \,, \tag{1}$$

calls for a smaller number of turns N or, equivalently, higher accelerating RF voltage per turn V_{RF} – see Fig.2.

Arrangement of coherent beam oscillations and use of a local shift of the radial betatron frequency further help to enhance the last turn separation and allow, e.g., 99.98 % operational extraction efficiency of the record high beam power of 1.4 MW average power in the PSI proton cyclotron [12].

There is also an effort to understand whether acceleration of H_2^+ ions, rather than protons or H^- particles, could allow the reduction of the space-charge induced losses and increase maximum current in a cyclotron [13].

1.3 Synchrotrons

Beam losses and emittance growth usually set operational limits on the maximum beam intensity and brightness in accumulator rings and proton synchrotrons [4, 16]. The need to keep the uncontrolled radiation level in accelerator enclosures of high power rapid-cycling synchrotrons (RCSs) $W = f_0 \int E_k dN_p$ under 1 W per meter of circumference C (here f_0 is the cycle rate and E_k is the kinetic energy of the lost particle) results in the tolerable fractional beam intensity loss of

$$\frac{\Delta N_p}{N_p} \leq \frac{W}{(1-\eta)N_p\langle E_k\rangle f_0}\,, \tag{2}$$

where η is the efficiency of the collimation system that directs the losses into dedicated beam absorbers or dumps. Unfortunately, the losses usually get bigger with the increase of beam intensity, energy and power – counter to the demand of Eq.(2).

Maximum performance is often based on the multi-turn charge-exchange injection by stripping H^- beams on thin foils or, recently, by lasers. Fractional beam losses at injection and extraction, though growing with the number of injection turns and, therefore, the total intensity, can be kept well under 1% by clearing the gaps intended for corresponding kicker pulses. Most detrimental effects occur over many turns of accumulation and acceleration (10^2 to 10^5), and are usually caused by a complex interplay of space-charge effects, coherent instabilities (dipole and higher order ones) in transverse and longitudinal planes, transition crossing, etc.

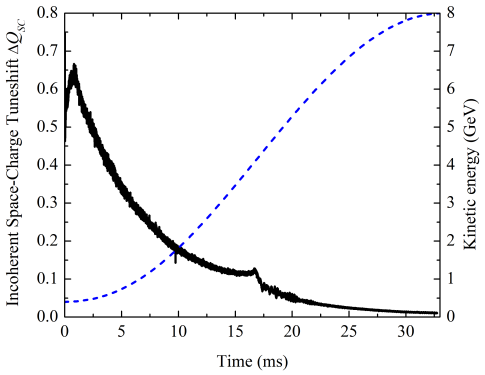

Figure 3: Time-dependent space-charge tuneshift parameter $\Delta Q_{sc}(t)$ (solid line) on the FNAL Booster energy ramp (dashed line).

	E_i/E_p	N_p	T	P	ΔQ_{sc}	$\%_{N_p}$	$\%_\epsilon$	C	S	$Q_{h,v}$
ISIS	0.07/0.80	3.1	0.01 s	200	0.4	2		163	10	4.31/3.83
PS-B	0.05/1.4	0.25	1.2	n/a*	0.50	5	20	157	16	4.3/4.45
CSNS	0.08/1.6	1.6	0.02	100	0.28	1	20	228	4	4.86/4.78
J-RCS	0.4/3	4.2	0.02	500	0.35	0.3	10	348	3	6.45/6.32
FNAL-B	0.4/8	0.45	0.03	84	0.60	5	20	474	24	6.78/6.88
CERN-PS	1.4/28	1.5	3.6	n/a*	0.24	3	5	628	50	6.12/6.24
JPARC-MR	3/30	27	1.5	515	0.4	1.5	10	1568	3	21.35/21.43
FNAL-MI	8/120	5.1	0.62	803	0.09	2.5	5	3319	1	26.46/25.38
CERN-SPS	28/450	0.9	19	n/a*	0.21	5	10	6911	6	20.13/20.18
PSR	0.8	3.1	6e-4	80	0.29	0.3		90	10	3.18/2.19
SNS-R	1	14	0.001	1400	0.15	0.01		248	4	6.23/6.20
FNAL-RR	8	5.2	0.84	54	0.09	2.5	10	3319	1	25.44/24.43

Table 1: Operational high intensity RCSs and ARs: injection/extraction kinetic energies E_i/E_p in GeV, number of protons per pulse N_p in 10^{13}, beam acceleration/storage time T in s, average beam power P in kW, maximum SC tune shift ΔQ_{sc}, fractional intensity loss $\%_{N_p} = \Delta N_p/N_p$ and emittance growth $\%_\epsilon = \Delta\epsilon/\epsilon$ in %, circumference C in m, lattice periodicity S and tunes $Q_{h,v}$. (* current LHC operation numbers. For the CNGS operation in 2005-2012, the SPS delivered $4.8 \cdot 10^{13}$ protons per pulse every 6 s, resulting in 510 kW average power at 400 GeV).

Space-charge tuneshift parameter ΔQ_{sc} is a commonly used figure of merit for beam dynamics [14, 15]:

$$\Delta Q_{sc} = \frac{N_p r_p B_f}{4\pi\varepsilon\beta_p\gamma_p^2} R\,, \tag{3}$$

where N_p is the total intensity, assuming that the bunches fill all RF buckets, r_p is the classical proton radius, B_f is the bunching factor (the ratio of the peak to average bunch current), ε is the normalized rms beam emittance, and β_p and γ_p are relativistic Lorentz factors. Factor $R \leq 1$ accounts for unequal average beam size ratio around the ring. The tuneshift is negative, so all the machines set up their working point $Q_{h,v}$ above and between major detrimental resonances $lQ_h + mQ_v = nS$, where l, m, n are integers and S is effective periodicity of the focusing accelerator lattice. In operational circular rapid cycling accelerators, the space-charge parameter usually does not exceed 0.3-0.5 to avoid unacceptable beam losses, see Table 1. Because of acceleration, bunching, emittance blowup and loss of the intensity, the tuneshift parameter varies in time, usually emphasizing the strength of the space-charge effects early in the acceleration cycle – see Fig.3.

Space-charge induced losses usually scale non-linearly with beam intensity $\Delta N_p/N_p \propto \Delta Q_{sc}^\kappa$, with high power $\kappa \simeq 2-4$, and are highly sensitive to the tunes, chromaticities, available aperture, RF and longitudinal dynamics, and

other phenomena. Usually, more than one counter-measure needs to be employed to maintain the losses under the limit of Eq.(2), including [4, 16, 17]: i) proper choice and dynamic adjustment of the working point $Q_{h,v}$ - see Fig.4; ii) reduction of chromaticities $Q'_{h,v}$ to the level allowed by coherent instabilities, such as electron cloud (*ep*) and/or due to impedance, and the feedback dampers; iii) lattice corrections to maintain the symmetry S and/or suppress the strength of the most dangerous resonances; iv) opening up the aperture to the maximum possible; v) improving the halo collimation efficiency η; vi) employment of the 2nd or higher harmonic RF system to reduce the bunching factor B_f; vii) injection painting to generate uniform initial transverse and/or longitudinal charge distributions leading to linearization of the space-charger forces [18], and, where possible, viii) increase the injection energy. Under active exploration are other advanced techniques, such as space-charge compensation using electron lenses - see [19] and Section 7.2.17, or implementation of the non-linear integrable optics [20].

Longitudinal dynamics and losses out of RF buckets are also of serious concern, especially for high-intensity machines whose operation involves slip-stacking, RF gymnastics and/or the transition crossing. For example, given that the transition energy $\gamma_t = \sqrt{1/\alpha_p} \simeq Q_h$ is usually much higher than the injection one, the limit on the fractional beam losses due to complicated 3D dynamics at transition, including transverse and longitudinal coherent instabilities, is very tight. Fast tune variation (γ_t jumps), RF manipulations and feedback, and other methods to keep the phenomena under control are described in Sec. 4.9.

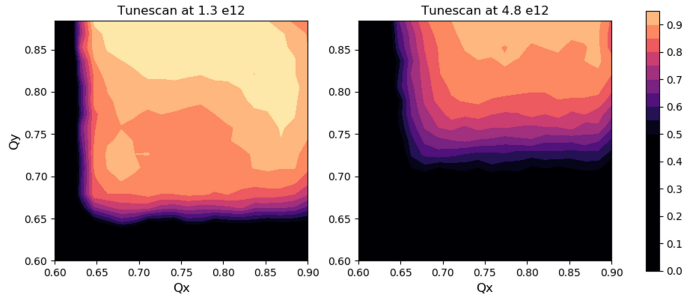

Figure 4: Tune scans of the Fermilab Booster transmission efficiency over the first 1 ms (∼1000 turns) after injection: (left) at low intensity of $N_p = 1.3 \cdot 10^{12}$ protons per batch and $Q'_{h,v}$=-20/-20, and (right) at high intensity $N_p = 4.8 \cdot 10^{12}$ at the same chromaticity (Booster operates at $N_p = 4.3 \cdot 10^{12}$, $Q_{h,v} = 6.78/6.88$ and $Q'_{h,v}$=-16/-4).

References

[1] V. Lebedev, V. Shiltsev, eds., Accelerator physics at the Tevatron collider (Springer, 2012)

[2] T. Wangler, Principles of RF Linear Accelerators (Wiley, New York, 1998).

[3] T. Stammbach et al, NIM-B, 113 (1996) 1

[4] J. Wei, Rev.Mod.Phys. 75 (2003) 1383

[5] I. Strasík, E. Mustafin, M. Pavlovc, PRAB 13 (2010) 071004

[6] P. Ostroumov, F.Gerigk, RAST 6 (2014) 171

[7] L. Groening, et al, PRL 102 (2009) 234801

[8] I. Hofmann, Space charge physics for particle accelerators (Springer, 2017)

[9] R. Gluckstern, PRL 73 (1994) 1247 (1994).

[10] M. Schuh, et al, PRAB 14 (2011) 051001

[11] W. Joho, 1981 Int'l Conf. Cyclotrons (Caen, France), 337; R. Baartman, Cyclotrons'2013 (Vancouver), 151

[12] M. Seidel, CERN-2018-008-SB, 151

[13] D. Winklehner et al, arXiv:2103.09352

[14] D. Lichtenberg, MURA-208 (1956)

[15] M. Reiser, Theory and design of charged particle beams (Wiley-VCH, 2008).

[16] J. Tang, Rev.Accel.Sci.Tech. 6 (2013) 143

[17] J. Eldred, et al, PRAB 24 (2021) 044001

[18] H. Hotchi et al, PRAB 20 (2017) 060402

[19] Yu. Alexahin, V. Kapin, JINST 16 (2021) P03049

[20] S. Nagaitsev, et al, JINST 16 (2021) P03047

2 BEAM-BEAM COMPENSATION SCHEMES

V.Shiltsev, FNAL
G.Sterbini, CERN

Significant experimental advances on beam-beam compensation have been made in the past decade. The perturbative or disruptive effect of the beam-beam interactions (see Sec.2.5) is indeed a basic limitation to increasing the luminosity of colliders and there is a strong incentive to devise and study compensation methods. With the advent of hadron colliders with a small bunch spacing, it becomes necessary to consider the compensation of both the head-on and the long-range beam-beam effects. By nature, the head-on beam-beam force derives from a Poissonian potential while the forces of traditional beam optics magnets are Laplacian, defeating attempts at correcting one by the others, at least exactly. The long-range beam-beam effect is, however, close to Laplacian for realistic beam-beam separations, opening new compensation possibilities.

2.1 Compensation of the head-on beam-beam effect

Four-beam compensation If four beams are made to collide at the same point, with, for each direction of propagation, one beam of particles and one beam of antiparticles of equal intensity and transverse beam sizes, there is no net electromagnetic beam-beam force. This concept was experimented in DCI (e^+/e^- at 0.8 GeV beam energy) [1]. While in a three-beam weak-strong configuration, an increase by a factor of 5 of the beam-beam limit was observed, no improvement of performance was obtained in the four beam configuration [2]. Unexpected excitation of non-linear beam-beam resonances was noticed, as well as coherent signals. These observations are in agreement with predicted loss of beam stability in the four-beam system, both for dipole [3] and for higher order modes of coherent motion [4]. Simulations of the four-beam compensation in linear e^+e^- colliders also indicate instabilities, which lead to significant separation of two beams and luminosity reduction even at very small initial bunch displacement errors [5, 6].

Electron-lens compensation The compensation of the beam-beam effect by an auxiliary beam is a variation of the above solution that allows a drastic simplification appropriate for high-energy colliders, with some limitations. An auxiliary electron beam of low energy is prepared in a source, made to collide with the main beam in a strong solenoidal field and dumped after the interaction, suppressing the possibility of coherent coupling, suspected to have plagued the four-beam concept. The auxiliary beam shall have suitable charge/direction of propagation for compensation and the same transverse positions and sizes as the perturbing beam [7]. It should ideally be positioned at the interaction point. This is, however, not possible in practice, and mitigations must be carried out in the compensation strategy. The first studies and successful use of electron lenses for the beam-beam compensation were done at the Tevatron $p\bar{p}$ collider (see Sec.7.2.17), with a schematic view of the lens). The primary beam-beam

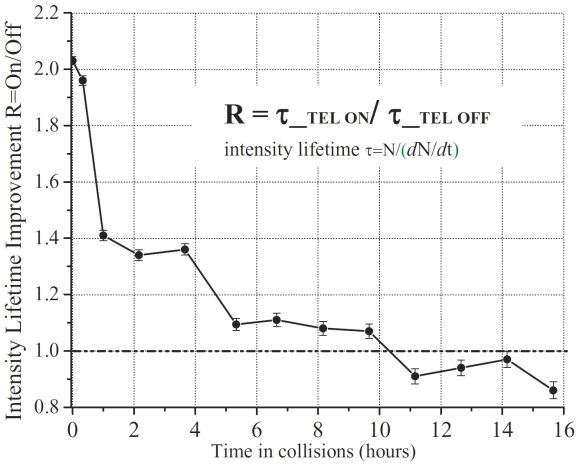

Figure 5: Improvement of the intensity lifetime of the Tevatron proton bunch 12 with TEL switched on, from [8].

limitation of the Tevatron performance was related to the tune spread along the bunch train induced by long-range beam-beam interactions. By using electron lenses as pulsed bunch-by-bunch focusing elements, the tunes of the normal and pacman bunches can be equalized, leading to a two-fold lifetime improvement [8] - see Fig.5). Comprehensive tests helped to optimize the transverse electron current density for linear corrections (constant electron density over the main beam extent and smooth tails) and have successfully demonstrated the high reliability and compatibility of electron lenses with the operation of superconducting hadron colliders. It was shown that the noise of the electron current can be reduced to a level that does not cause emittance blow-up of the main beams [8] .

Successful non-linear beam-beam compensation by Gaussian electron lenses has been demonstrated in RHIC. The collider luminosity in polarized proton operation was severely limited by the head-on effect. In 2015, partial, half-strength compensation of the head-on beam–beam effect with two electron lenses installed in RHIC (one for each proton ring), together with the proton intensity and emittance and the collider optics upgrades, approximately doubled the peak and average luminosities [9]. To compensate both the tune spread and the beam-beam generated resonances, the RHIC electron lenses were placed at a betatron phase advance of a multiple of π from the main IPs (Fig.6), they had a matching electron current and the same transverse rms electron beam size as the proton one (about 0.6 mm), and allowed accurate relative positioning of both beams and their overlap within a fraction of the rms size. While in prior polarized proton collider runs strong emittance growth had limited the peak collider luminosity at the level corresponding to a beam-beam parameter per IP of $\xi_p = 0.006$, in 2015, with the electron lenses, the beam-beam parameter of 0.011 per IP

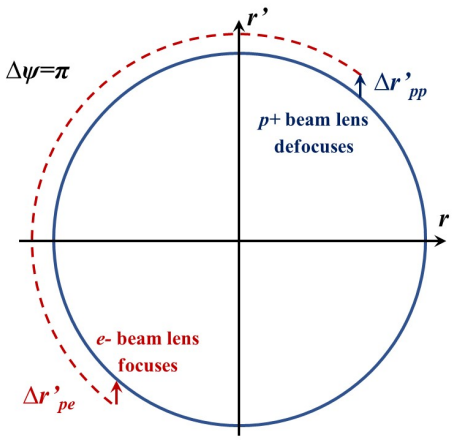

Figure 6: Head-on beam-beam compensation in a phase space view. A defocusing kick $\Delta r'_{pp}$ a proton receives from the other proton beam is reversed by a focusing kick $\Delta r'_{pe}$ from the electron lens after a phase advance π.

had been routinely achieved without the large emittance growth. The proton tune distribution measurements with a transverse beam transfer function system confirmed substantial (about two-fold) reduction of the beam-beam tunespread by the electron lenses – see Fig.7).

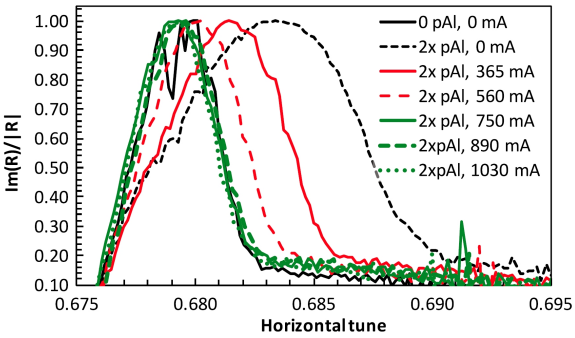

Figure 7: Tune distribution width reduction with the RHIC electron lens, measured in the proton beam with p+Al collisions. The distribution widens due to two beam-beam interactions, and narrows again with increase of the electron lens current to 1.03 A [9].

Compensation by octupoles In VEPP-4 (e^+/e^- at 5.3 GeV), the compensation of the cubic beam-beam non-linearity using octupoles was systematically investigated by scanning the tune plane and the lattice octupole strength [10]. Although a several-fold reduction of electron halo loss rate was demonstrated

at optimal octupole current, no clear improvement could be obtained under operating conditions in VEPP-4 or in CESR, where similar trials were made.

Successful application of octupoles to compensate parasitic beam-beam interaction effects was demonstrated in DAΦFNE (INFN, Frascati) for different collider configurations. In particular, by tuning the working point and the strength of an electromagnetic octupole consistently with nonlinearities compensation, the positron beam lifetime was doubled when the opposite electron beam had the maximum current [11].

Parasitic beam-beam compensation using the arc octupoles was also successfully demonstrated in the LHC [12].

Advanced optics Cancellation or significant reduction of beam-beam resonances, and, therefore, increase of the beam-beam limit, occurs in advanced beam optics schemes, such as "round colliding beams" and the "crab-waist crossing" (see Secs.2.5.2, 4.13). Also, in colliders where the beams collide at several points, it is possible to phase these points so as to self-compensate certain resonant non-linear terms chosen or observed to be most harmful for the performance. For example [13], in the case of two identical collision points, all beam-beam resonances of order N can be canceled by choosing a betatron phase advance between collision points $\Delta\Phi_x = \Delta\Phi_y = 2\pi(p/N + q)$, p, q, N integers with p odd. Detuning terms that are not phase-dependent will not be suppressed. The concept awaits experimental confirmation.

2.2 Compensation of the long-range beam-beam effect

Alternate crossing planes at pairs of collision points It was recognized in [14] that crossings at pairs of identical interaction regions alternately in horizontal and vertical planes cancel the linear long-range beam-beam tune shifts. For sufficient beam separation where the perturbing beam can be well modeled by a wire, the magnetic field expansion is given by:

$$B_y + iB_x = \frac{\mu_0 I_b}{2\pi r_0} \sum_{n=1}^{\infty} (b_n + ia_n) \left(\frac{x+iy}{r_0} \right)^{n-1} \tag{4}$$

$$\text{with} \quad (b_n + ia_n) = -\cos(n\Phi) - i\sin(n\Phi)\,;$$

I_b is the beam current, r_0 the beam separation, $\Phi = 0$ for horizontal separation and $\Phi = \pi/2$ for vertical separation. One can note that the gradient coefficient b_2 driving the linear tune shift changes sign from horizontal to vertical crossing. This is true for both normal and pacman bunches, which would otherwise experience different long-range beam-beam tune shifts. Hence, alternate crossings effectively reduce the beam tune footprint. This cancellation depends on the multipole order and is not true in general. Alternate crossings excite beam-beam resonances in both planes, reducing the space available for the beam footprint in the tune plane. In simulations, e.g. [15], its benefit is not really determinable and experimental data are needed to assess the actual efficiency of this compensation method.

Wire compensation The principle of an almost exact compensation of the long-range beam-beam effect with wires was proposed in [16] for the LHC, where the long-range beam-beam interactions are clustered on either side of the interaction points. With two wires per interaction region and per beam, efficient compensation requires small betatron phase advance between clustered perturbations and compensation (a few degrees); the same transverse beam aspect ratio as at the long-range perturbations; beam-wire separation identical to the beam-beam separation at the long-range interaction points when expressed in units of rms transverse size; integrated wire current equal to the sum of integrated beam currents in the cluster; the wires should be positioned in a location where the separation between the beam channels allows to install the movable wire set-up and their distance with the beam should remain compliant with the machine protection requirements.

DC wire experimental program was conducted in the LHC [17]. The experiment proved the efficiency of the wire compensation for regular bunches (with the maximum number of parasitic encounters) and the absence of detrimental effects on the super-pacman bunches (without parasitic encounters). The results of the compensation experiment are summarized in Fig. 8 where the proton losses normalized with respect to the total luminosity of the collider are shown as function of the wire currents. For optimal beam lifetime, this observable corresponds to ≈ 80 mbarn, e.g. the pp inelastic cross-section at 6.5 TeV. When the wire compensation is active, the beam losses of the regular bunch are almost halved and reduced to the luminosity burn-off limit, preserving, in the meantime, the lifetime of the super-pacman bunch. For HL-LHC, a method to optimize the wire current and position compatible with the HL-LHC beta-leveling strategy was proposed [18].

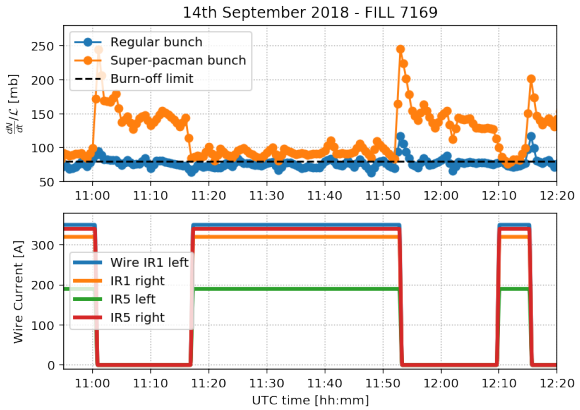

Figure 8: Beam-beam long-range wire compensation effect on a regular and super-pacman bunch in LHC (top) together with the current of the four wire compensators (bottom) [17].

Dedicated beam studies with DC wire long-range beam-beam compensation

proper were carried out in RHIC and also showed evidence of the compensation [19].

If the long-range beam-beam interactions are not clustered but distributed all around the machine, wire compensation meets the same difficulties as non-local non-linear corrections [20]. On the other hand, for DAΦNE (INFN, Frascati), a non-local wire correction was successfully implemented, leading to a significant increase of the beam and luminosity lifetimes (Fig.9) – in a good agreement with the 3D numerical simulations of beam-beam interaction in the collider nonlinear lattice [21].

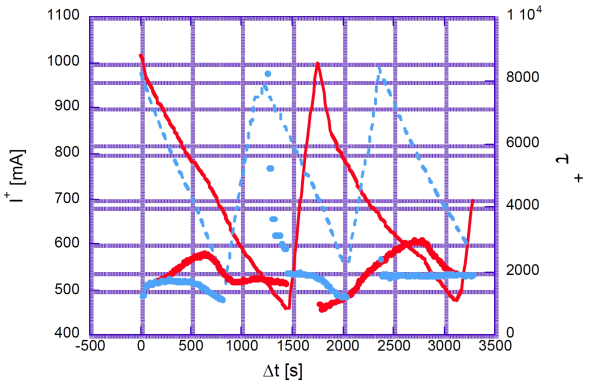

Figure 9: DAΦNE positron current and lifetime as a function of time: wires on (red) and wires off (cyan) [21].

Compensation by multipoles For non-local non-linear corrections, magnetic multipoles can be an alternative. A global approach proposed in [22] relies on a minimization of the nonlinearities of the one-turn map up to order 6 in the Hamiltonian, using magnetic multipoles in the machine arcs. It is shown, in a case close to that of the nominal LHC, that the correction allows recovery of most of the 40% of dynamic aperture lost due to the beam-beam effect (long-range and head-on).

References

[1] J. Augustin et al, HEACC 69 (Yerevan), v.2, 113

[2] J. Le Duff, M. Level, LAL-RT-80-03 (Orsay, 1980)

[3] Ya. Derbenev, SLAC TRANS-151 (1973)

[4] B. Podobedov, R. Siemann, PRE 52, 3066 (1994)

[5] V. Balakin, N. Solyak, HEACC 86 (Novosibirsk), v.1, 151

[6] D. Whittum, R. Siemann, PAC 97, 602

[7] E. Tsyganov et al, SSCL-519 (1993); V.Shiltsev et al, PRSTAB 2, 071001 (1999).

[8] W. Shiltsev et al, PRL 99, 244801 (2007); NJP 10, 043042 (2008)

[9] W. Fischer et al, PRL 115, 264801 (2015); PRAB 20, 091001 (2017)

[10] A. Temnykh, Proc. 3^{rd} Adv. ICFA Beam Dynamics Workshop, Novosibirsk (1989), 5

[11] M. Zobov, ICFA BD NL 31, 14 (2003); C. Milardi et al, arxiv:0803.1544

[12] S. Fartoukh et al, PRAB 24, 021002 (2021)

[13] S. Peggs, Proc. Workshop on AP Issues for SSC, UM HE 84-1 (1984) 58

[14] D. Neuffer, S. Peggs, SSC-63 (1986)

[15] F. Zimmermann, EPAC 04, 83

[16] J.-P. Koutchouk, LHC Project Note 223 (2000); PAC 01, 1681

[17] G. Sterbini et al, IPAC 19, 2262

[18] S. Fartoukh et al, PRST-AB 18, 121001 (2015)

[19] R. Calaga et al, PRST-AB 14, 091001 (2011)

[20] T. Sen, B. Erdelyi, PAC 05, 2645

[21] C. Milardi et al, EPAC 06, 2808; A. Valishev et al, IPAC15, 589

[22] J. Shi, L. Jin, O. Kheawpum, PR E69, 036502 (2004)

3 SPACE CHARGE COMPENSATION (SCC) IN HADRON BEAMS

V. Shiltsev, FNAL

3.1 Longitudinal SCC: Inductive Inserts

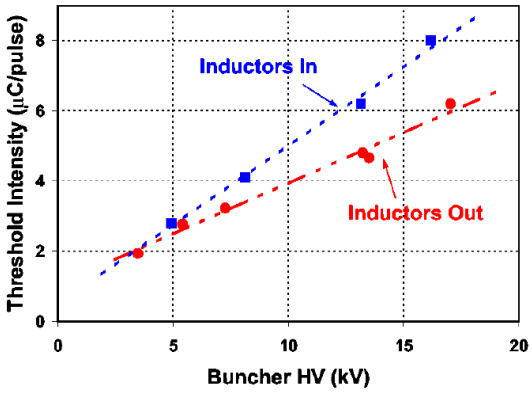

Figure 10: PSR *e-p* instability threshold vs rf buncher voltage with and without inductive inserts.

Longitudinal space-charge fields can generate substantial distortion of the rf-generated potential wells, fill the extraction kicker gap in the beam, affect the incoherent synchrotron tune spread, and have the potential for causing instability and longitudinal emittance growth (also see Sec.2.4.5.1). The net effective voltage per turn resulting from the space-charge self voltage and the ring inductive wall impedance $\omega_0 L$ is proportional to the slope of the beam current distribution $e\beta c\lambda(s)$ and can be expressed as:

$$V_s = \frac{\partial \lambda(s)}{\partial s}\left[\frac{g_0 Z_0}{2\beta\gamma^2} - \omega_0 L\right] e\beta c R$$

where $R = c/\omega_0$ is the average machine radius, $Z_0 = 377$ Ohm and $g_0 = 1 + 2ln(b/a)$ is the geometric space-charge constant, a and b are the beam radii and vacuum-chamber aperture. By introducing a tunable inductance L, e.g., ferrite rings, the term in brackets and, consequently, the space-charge effect may be substantially reduced or canceled at some chosen energy [1].

This concept has been experimentally proven at the LANL Proton Storage Ring at LANL where three inductive inserts, each consisting of 30 "cores" of a cylindrically shaped ferrite with a thickness of 1 inch, an inner diameter of 5 inches, and an outer diameter of 8 inches, were installed. The magnetic permeability of the ferrite could be adjusted by introducing current into solenoids

wound around the ferrite so that in the MHz range of frequencies the longitudinal space charge impedance of the machine was compensated [2]. A strong longitudinal instability was noticed at much higher frequencies of about 75 MHz, but it was later suppressed by heating the ferrite to a temperature of 130°C to make it lossier.

The inserts have proven beneficial in raising the threshold for the two-stream e-p instability at PSR (Fig.10) and achieving shorter bunch length.

3.2 Transverse SCC

There are several methods to compensate transverse s.-c. effects, which often manifest themselves in the form of beam loss, core emittance growth, and halo formation (also see Sec.X.Y.Z).

Passive cancellation of the next-to-leading term in the s.-c. force is possible by **octupole** fields. For a round beam, the 4th order of term of the direct s.-c. potential varies as $(x^4 + 2x^2y^2 + y^4)$, while the potential of an octupole is proportional to $(x^4 - 6x^2y^2 + y^4)$. Therefore, at least two families of octupoles are needed to reduce the s.-c. tune spread, which are placed at locations with either peak and intermediate values of the beta function, respectively. The beta functions should sufficiently vary over the length of an optical cell, e.g., by a factor 2 or more.

Pole-face windings allow precise adjustments of the tune shift with transverse position up to a high order. At the CERN ISR, 24 pole-face windings modifying the local magnetic field were used to correct the horizontal and vertical indirect s.-c. tune shift plus the next 4 orders in their Taylor expansions with respect to the horizontal position. The correction increased the maximum ISR beam current 15 times [3].

Nonlinear integrable optics, which could accommodate extraordinary large tune spreads in circulating beams without driving resonant losses, also show promise for the s.-c. dominated beams [4].

In the case of **passive neutralization**, the s.-c. force of a proton beam can be compensated by ionization electrons, electron cloud, or negative ions, which are approximately at rest longitudinally, but move transversely during the beam passage. The fraction of negative charge needed for compensation is $\eta \approx 1/\gamma_p^2$. Accumulated ionization electrons produced by the primary beams are effectively used in neutralized low energy beam transport (LEBT) lines [5]. A factor of 9.5 increase of the maximum circulating beam current above (coherent) s.-c. limit was achieved at the Novosibirsk 1 MeV proton ring by increasing the residual gas pressure in excess of 10^{-4} Torr and accumulation of ionization electrons [6]. The beam lifetime was very short and transverse and longitudinal proton distributions were not well controlled.

Optimum SCC requires that the transverse electron and proton beam distributions are matched. That could be achieved by confining the electrons transversely with strong solenoid fields to "columns" and using electrostatic electrodes to fine-tune the charge density. Strong magnetic field also stabilizes electron "column" motion and prevents coherent *e-p* instability. Simulations

show significant reduction of the s.-c. induced emittance growth with only a few "columns" occupying a small fraction of the ring circumference [7].

Electron lenses, in which externally generated strongly magnetized electron beam with matched transverse distribution collides with the proton beam inside a strong solenoid field (see Sec.7.2.17), could also be employed for the SCC. Assuming N_l electron lenses, each of length l, distributed around the ring, and electron beams co-propagating with the beam of N_p protons, the needed maximum electron current in each lens is [8]

$$J_e = \kappa B_f \frac{ecN_p}{N_l l} \frac{\beta_e}{\gamma_p^2(1-\beta_p\beta_e)}$$

and for many accelerators of interest lies in the range of 1-10A for 10-40 keV electrons (here κ denotes the degree of compensation; B_f is the ratio of the peak to average proton bunch current, $\beta_{e,p}, \gamma_p$ are electron and proton relativistic Lorentz factors). Besides the transverse profile matching, effective SCC for very high brightness hadron beams with ΔQ_{SC} approaching -1.0 requires: a) electron current to be modulated to match longitudinal profile of hadron bunches, b) several weaker (rather then one strong) electron lenses around, i.e., N_l either equal to the ring lattice periodicity $P \gg 1$ or being one its factors, c) incomplete degree of compensation $\kappa = 0.5 - 0.75$ [9, 10, 11]. Experimental developments toward the SCC with electron lenses are underway for the IOTA ring at Fermilab [12] and for the SIS18 synchrotron at GSI [13].

References

[1] R.J. Briggs, V.K. Neil, J.Nucl.Energy, Part C 8 (1966) 255

[2] M.A. Plum et al, PRST-AB 2 (1999) 064201

[3] P.J. Bryant et al, CERN ISR-MA/75-54 (1975)

[4] S. Nagaitsev, JINST 16 (2021) P03047

[5] B. Logan et al, Nucl.Fusion, 45 (2005) 131

[6] G. Dimov, V. Chupriyanov, PA 14 (1984) 155

[7] V. Shiltsev et al, AIP Conf. Proc. 1086 (2009) 649

[8] A. Burov, G. Foster, V. Shiltsev, FNAL-TM-2125 (2000)

[9] M. Aiba et al, PAC 07, 3390

[10] O. Boine-Frankenheim, W. Stem, NIMA 896 (2018) 122

[11] E. Stern et al, JINST 16 (2021) P03045

[12] G. Stancari et al, JINST 16 (2021) Pxxxxx

[13] S. Artikova et al, JINST 16 (2021) P03044

4 Electron Lenses

V. Shiltsev, FNAL

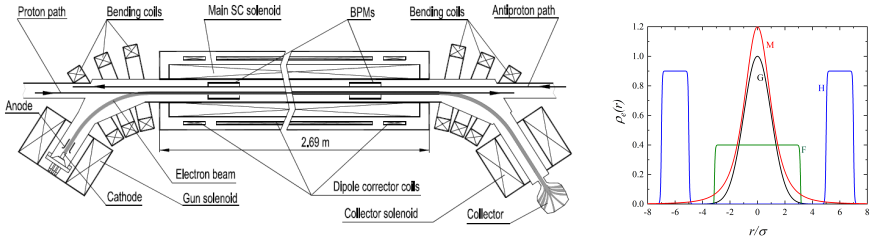

Figure 11: (left) General layout of the Tevatron electron lens; (right) transverse electron current profiles: (G) Gaussian for space-charge and head-on beam-beam compensation, (F) flat-top for bunch-by-bunch tune spread compensation, (H) hollow beam for halo collimation, and (M) McMillan shape for integrable optics.

Electron lenses employ EM fields of low-energy, high-intensity electron beams colliding with the bunches of high-energy particles, e.g., protons, antiprotons, electrons, or ions, over an extended length (see [1] and references therein). Strongly magnetized electron beams can be produced in a variety of shapes and time structures as needed for such applications as compensation of beam-beam and space-charge effects [2, 3, 4] (see Sec.4.14 and Sec.4.15), beam halo collimation [4], Landau damping [5] or integrable optics [6].

The flexibility and broad spectrum of applications of electron lenses are due to their unique advantages, such as: a) electron beams are essentially transparent to high-energy beams as they act only through EM forces, with no nuclear interactions; b) electron beam space charge can generate very strong fields $O(1$ MV/m), which are very localized in space – they fall as $1/r$ outside the characteristic beam radius $r > a_e$; c) transverse electron beam size and current profile $j_e(r)$ and, thus, the EM field profiles can be arranged in a variety of shapes – for example, Gaussian, flat-top, hollow, etc., as depicted in Fig.11 – by shaping the electron gun cathode and extraction electrodes; d) the electron lens current can be varied quickly on very fast time scales $O(10$ ns), opening opportunities for applications that require not only DC impacts, but also pulsed, modulated, random, or periodic ones, which can be synchronized with individual high-energy bunches or subsets of bunches and provide highly selective effects for each subset; e) in a typical electron lens configuration, electrons are produced at the cathode of an electron gun and get damped in a collector right after passing the interaction area; thus, fresh electrons interact with the high-energy particles on each turn, leaving no possibility for coherent instabilities.

The first electron lenses were installed in the Tevatron p-$\bar{p}$ collider [8] – see Fig.11 – and used for compensation of the long-range beam-beam effects [9], beam halo collimation [5] and operational abort gap beam removal [10]. Up to 3 A, 6-10 kV electron beams were generated at the 10-24 mm diameter

thermocathodes immersed in 0.3T longitudinal magnetic field and aligned onto (anti)proton beam orbit over a length of about 2 m inside 6 T SC solenoids. Electron pulses of 60-600 ns were generated by changing electron gun anode voltage at the repetition rate of 48 kHz. Later, two electron lenses were built for the RHIC *p*-*p* operations and effectively employed for head-on beam-beam compensation [11] and as hollow electron beam collimators. New electron lenses are being designed for the space-charge compensation in the IOTA ring at Fermilab [12] and SIS18 synchrotron at GSI [13], as well as for the high-luminosity LHC beam collimation [14] – see table of their main parameters, such as length L_e in meters, maximum solenoid magnetic field B[T], electron beam voltage U_e[kV], maximum current J_e[A], characteristic beam size a_e[mm] and current density profiles.

e-lens	L_e	B	U_e	J_e	a_e	profile
Tevatron	2.0	6	10	3	$\sim$2	F, G, H
RHIC	2.1	3	5	1	0.6-2.4	G, H
IOTA	0.7	0.8	10	3	15	G, M
LHC	3.0	5	15	5	1-2.2	H
SIS18	3.4	0.6	30	10	25	G

References

[1] V. Shiltsev, Electron Lenses for Super-Colliders (Springer, 2016).

[2] E. Tsyganov et al, SSCL-519 (1993)

[3] V. Shiltsev, et al, PRST AB 2 (1999) 071001

[4] A. Burov, G. Foster, V. Shiltsev, FNAL-TM-2125 (2000)

[5] G. Stancari et al, PRL 107 (2011) 084802

[6] V. Shiltsev et al, PRL 119 (2017) 134802

[7] V. Danilov, V. Shiltsev, JINST 16 (2021) P03050

[8] V. Shiltsev et al, PRST AB 11 (2008) 103501

[9] V. Shiltsev et al, PRL 99 (2007) 244801

[10] X.-L. Zhang et al, PRST AB 11 (2008) 051002

[11] W. Fischer et al, PRL 115 (2015) 264801

[12] S. Antipov et al, JINST 12 (2017) T03002

[13] S. Artikova et al, JINST 16 (2021) P03044

[14] S. Redaelli et al, JINST 19 (2021) P03042